New Design of Cylindrical Capacitive Sensor for On-line Precision Control of AMB Spindle

Soo Jeon
soojeon@amed.snu.ac.kr
Hyeong-Joon Ahn
ahj@amed.snu.ac.kr
Dong-Chul Han
dchan@amed.snu.ac.kr
School of Mechanical and Aerospace Engineering, Seoul National University, Korea

ABSTRACT
A new design of cylindrical capacitive sensor (CCS) for the displacement measurement of precision active magnetic bearing (AMB) spindle is presented in this paper. This research is motivated by the problem that existing 4-segment CCS is still sensitive to the 3rd harmonic component of the geometric errors of a rotor. The procedure of designing new CCS starts from modeling and the error analysis of CCS. The angular size of CCS is set up as a design parameter, and new 8-segment CCS is introduced to possess an arbitrary angular size. The optimum geometry of CCS to minimize the effect of geometric errors is determined through minimum norm approach. Experimental results with test rotors have confirmed the improvement in geometric error suppression.
Keywords : Cylindrical capacitive sensor, Geometric error, Active magnetic bearing

INTRODUCTION

Active magnetic bearings (AMB) levitate a rotor with feedback control of measured displacement sensor signal. The performance of AMB system is therefore directly affected by the quality of a sensor signal. Especially in precision applications such as machine tool spindles, it is essential to minimize the effects of geometric errors of rotor which cause serious vibration in AMB system.
The probe type displacement sensors most widely used in AMB system are very sensitive to surface quality of a rotor, so they require additional algorithms to detect and compensate the unnecessary signal induced by the geometric errors of a rotor [1] [2]. Accordingly, on-line control system with the probe type sensors becomes more bothersome and more complicated as high precision is required.
Cylindrical capacitive sensor (CCS) had been originally introduced by Chapman [3] for its advantages, which are the insensitivity to the geometric error by spatial averaging and high resolution with large sensing area. Chang [4] had compared the measuring processes of CCS with those of probe sensors through numerical simulation. Ahn [5] had analyzed the mechanical errors of CCS mathematically, and showed that CCS is superior to the probe type sensor in rejecting the geometric errors of a rotor. However, CCS is still sensitive to the odd harmonic components of the geometric errors, especially to the 3rd harmonic one. This is because the CCS is designed only to have the highest resolution with the largest sensing area without considering the minimization of the effects of geometric errors.
This paper proposes a new design of CCS based on the mathematical derivation of its measuring process. We introduce a new 8-segment CCS, which can possess an arbitrary angular size and reject one odd harmonic component of geometric errors by changing its angular size. The optimal angular size of CCS is determined through minimizing 1-norm of the non-dimensional measurement error or the error amplification factor. Experiments with test rotors are performed to confirm the effectiveness of the new design.

MODELING AND ANALYSIS

Cylindrical Capacitive Sensor

Capacitive sensors are widely used in short range ultra-precision and control applications because they have higher resolution than other type sensors. The greater the ratio of the area of sensor to the distance from target, the greater the accuracy and resolution of the sensor. In addition, the ratio of sensor area to the characteristic surface finish dimension of the part should be as great as possible to provide the averaging effect [6].

Therefore, the 4-segment CCS is designed to possess the largest sensing area and to use a differential configuration for stability to environmental changes, as shown in Fig. 1 a). The displacements X, Y of a rotor can be approximated with Eq. (1) of capacities of 4 sensing electrodes (C_1, C_2, C_3, C_4).

$$X = gain(C_1 + C_4 - C_2 - C_3), \quad Y = gain(C_1 + C_2 - C_3 - C_4) \tag{1}$$

The existing 4-segment CCS is composed of 4 sensing electrodes, a guarding electrode, and an epoxy resin for insulation, as shown in Fig. 1 b).

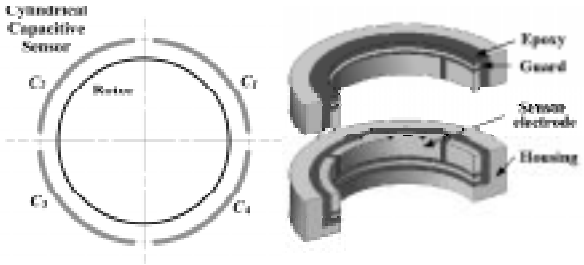

a) Configuration b) Elements

FIGURE 1: Conventional CCS

Mathematical Description of CCS

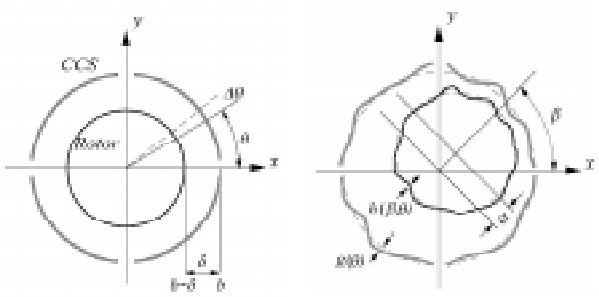

a) Ideal case b) Eccentric case with roundness errors

FIGURE 2: Variables for Small Capacitance

In order to determine design parameters of CCS, mathematical description of CCS [5], [7] is reviewed. When variables for the displacement measurement of CCS is given in Fig. 2, the small capacitance between the sensor and the rotor considering their geometric errors can be approximated as

$$\Delta C = \varepsilon \frac{b\Delta\theta w}{\delta - \alpha\cos(\theta - \beta) - h - g} \tag{2}$$

where b is the radius of the sensor, δ is the gap between the sensor and the rotor, $\Delta\theta$ is small sensor angle, ε is the dielectric constant, w is the axial length of CCS, and h and g are geometric errors of the rotor and the sensor respectively.

Introducing harmonic number m and phase angles γ and ϕ, the roundness errors of the rotor and the sensor can be modeled with Fourier series as follows.

$$h = \sum_{m=2}^{\infty} h_m \cos(m(\theta - \beta) + \gamma_m) \tag{3}$$

$$g = \sum_{m=2}^{\infty} g_m \cos(m(\theta - \beta) + \phi_m) \tag{4}$$

Since the effects of roundness errors of the rotor and the sensor are almost same, as shown in Eq. (2), only the effect of roundness errors of the rotor is investigated. Instead of using Eq. (2) in calculating capacities, Taylor series approximation is employed in that radius b is much larger than other variables α, δ.

$$\Delta C = \frac{\varepsilon b w}{\delta}\left(1 + \frac{\alpha}{\delta}\cos(\theta - \beta) + \frac{h}{\delta}\right)\Delta\theta \tag{5}$$

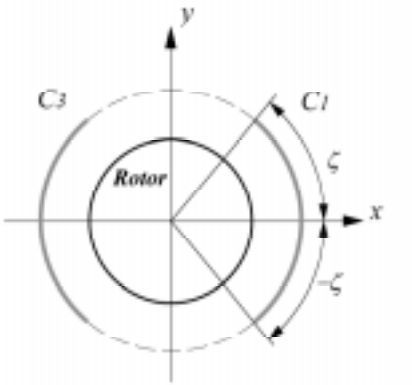

FIGURE 3: Angular Size ζ of CCS

Variable ζ for the angular size of CCS is introduced, as shown in Fig. 3. Then the measured rotor displacements are rewritten as

$$X = \int_{-\zeta}^{\zeta}\Delta C - \int_{\pi-\zeta}^{\pi+\zeta}\Delta C, \quad Y = \int_{\pi/2-\zeta}^{\pi/2+\zeta}\Delta C - \int_{3\pi/2-\zeta}^{3\pi/2+\zeta}\Delta C \tag{6}$$

When ζ approaches zero, the sensor becomes an ideal probe sensor. And it becomes an existing 4-segment CCS when ζ becomes 90°. In case of even harmonic error, the measurement error related to out of roundness is canceled during the integration of the Eq. (6). This means that the differential configuration eliminates even harmonic roundness errors regardless of sensor size. On the other hand, if m is odd, the displacement X of the rotor is given by the following equation.

$$X = \frac{4\varepsilon b w \sin\zeta}{\delta^2}\left\{\alpha\cos\beta - \sum\frac{h_m}{m\sin\zeta}\sin m\zeta\cos(m\beta + \gamma_m)\right\} \tag{7}$$

where the coefficient of the brace is equivalent to the gain of the sensor, the first term in the brace is the exact X displacement of the rotor, and the second is related to the roundness error of the rotor. In order to see the effects of geometric errors quantitatively, error amplification factor is defined as follows.

$$\frac{e_m}{h_m}(\zeta) = \frac{\sin m\zeta}{m \sin \zeta} \quad (m = 3,5,7,...) \qquad (8)$$

The error amplification factor represents the non-dimensional measurement error of each harmonic component of geometric errors. The error amplification factor converges to one irrespective of the harmonic number m as ζ approaches zero. This means that the roundness errors remain undiminished in the measured signal of the probe type sensor. On the contrary, the error amplification factor is inversely proportional to the harmonic number m when ζ is 90°, i.e. the sensor behaves as a 4-segment CCS. This is called the spatial averaging effect that the error amplification factor decreases as the harmonic number m increases.

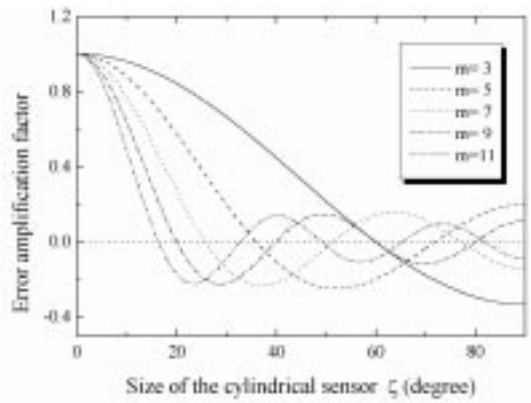

FIGURE 4: Error Amplification Factor with Various Odd Harmonic Numbers of m

Figure 4 displays the influence of angular size ζ on the error amplification factor e_h / h_m with various odd harmonic numbers. The arbitrary odd harmonic errors can be eliminated through adjusting the angular size ζ of CCS, as shown Fig. 4. The m^{th} harmonic error is rejected if the angular size of CCS satisfies the following equation.

$$m\zeta = n\pi, \quad 0^o \le \zeta \le 90^o \quad (n = 1,2,3,\cdots) \qquad (9)$$

For example, if the angular size ζ is 60°, 3rd harmonic error and its multiples are rejected. Similarly, to remove the 5th harmonic error and its multiples, angular size ζ may be chosen to be 36° or 72°, but 72° is recommended for the spatial averaging effect. It is also noticed from Eq. (9) that existing 4-segment CCS has the shape of removing 2nd harmonic component and its multiples. The configuration of 4-segment CCS is a redundant design because the even harmonic components are already suppressed through the differential configuration.

DESIGN

Sensor Configuration for Arbitrary Angular Size

The 4-segment CCS, as shown in Fig. 1 cannot possess an arbitrary angular size especially when the angular size ζ is larger than 45°. Consequently, authors propose a new 8-segment CCS, which consists of 4 shared segments and 4 unshared segments, as shown in Fig. 5. Total angular size 2ζ of the sensing unit is the sum of two shared segments and one unshared segment, as shown in Fig. 5.

$$2\zeta = 2S_S + S_U \qquad (10)$$

Also, the size of shared segment and unshared segment should satisfy the following constraint equation.

$$S_S + S_U = 90^o \qquad (11)$$

The new CCS can possess a discretionary angular size through changing angular sizes of the segments.

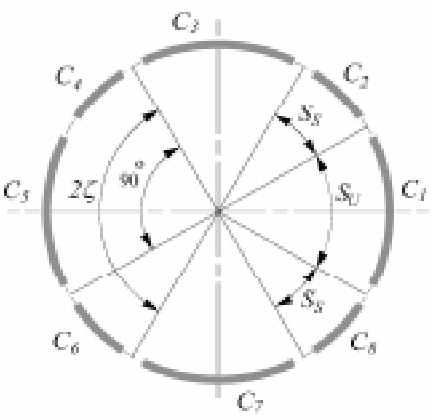

FIGURE 5: New 8 Segment CCS

Now the problem is which value of ζ is most suitable to minimize the effects of geometric errors. It is difficult to find out the optimal value of ζ in Fig. 4. In general, high harmonic components of geometric errors can be neglected because they are removed by the bandwidth of controller as well as by the spatial averaging effect. Among low harmonic components, the 3rd harmonic one in particular has the biggest amplification factor and more multiples than any other odd harmonic components. Also, the 2nd and 3rd harmonic components are the greatest and most prevalent harmonic components of roundness errors. Therefore, we can expect intuitively that the optimal angular size ζ of CCS is 60°, which eliminates 3rd harmonic component of roundness errors.

Optimization of Angular Size of CCS

Since actual geometric errors consist of various harmonic components, the sum of the various harmonic components should be considered to determine which value of ζ minimizes the effects of geometric errors. Correspondingly, 1-norm of the error amplification factor chosen as the cost function to be minimized.

$$F(\zeta) = \left\| W(m)\frac{e_m}{h_m}(m,\zeta) \right\|_1 = \sum_{m=3,5,..} \left| W(m)\frac{e_m}{h_m}(m,\zeta) \right| \quad (12)$$

where *W(m)* denotes a weighting function.

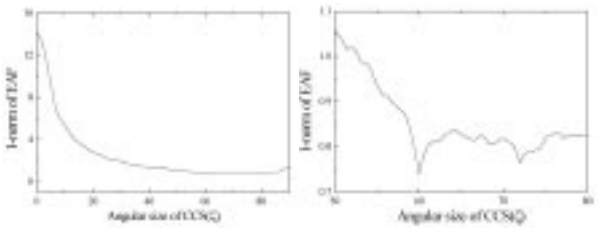

(a) ζ from 0° to 90° (b) ζ from 50° to 80°

FIGURE 6: 1-Norm of the Error Amplification Factor

Letting *W(m)* be 1 and allowing harmonic number *m* be up to 29, the calculated cost function $F(\zeta)$ and zoomed cost function $F(\zeta)$ in the range of ζ from 50° to 80° are shown in Fig. 6 a) and b) respectively. $F(\zeta)$ has the greatest value at ζ = 0° and tends to decrease as ζ increases. There is first rapid drop at 60° due to the elimination of 3rd harmonic component and the second small drop at 72° resulting from the elimination of 5th harmonic one. We can find in Fig. 6 b) that the cost function $F(\zeta)$ is minimized when angular size ζ is 60°.

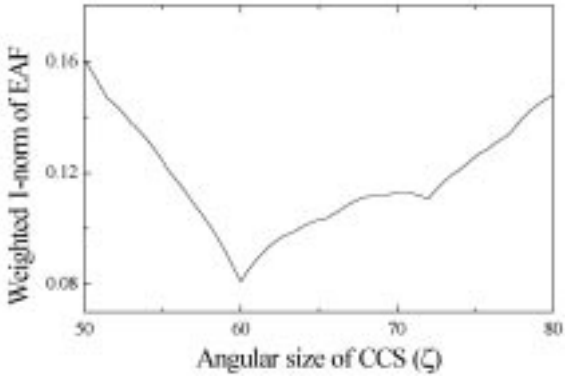

FIGURE 7: Weighted 1-Norm of Error Amplification Factor

The result above is the case in which all the harmonic components have equal magnitudes. But in an actual situation, the magnitudes of the harmonic components tend to decrease as the harmonic number increases. Therefore, the weighting function is chosen considering the dependency of magnitude of geometric error upon harmonic number. Figure 7 shows the calculated cost function $F(\zeta)$ when weighting function *W(m)* is 1 over *m*. The drop at 60° becomes more rapid and the optimal value is clearer than that in Fig. 6. As a result, the optimal angular size ζ is 60° to eliminate the 3rd harmonic component, as expected.

New CCS

If we choose angular size ζ to be 60°, the entire sensing unit takes up 120°. The configuration of the new CCS is shown in Fig. 8. The displacements *X,Y* of a rotor are approximated with Eq. (13).

$$\begin{aligned} X &= (C_8 + C_1 + C_2) - (C_4 + C_5 + C_6) \\ Y &= (C_2 + C_3 + C_4) - (C_6 + C_7 + C_8) \end{aligned} \quad (13)$$

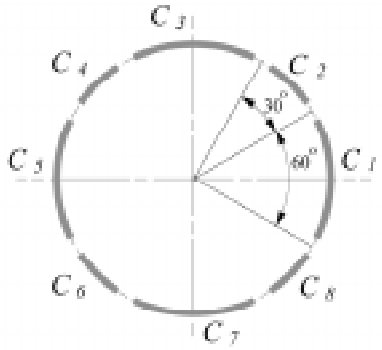

FIGURE 8: Optimal Design of CCS

EXPERIMENTAL RESULTS

Experimental Setup

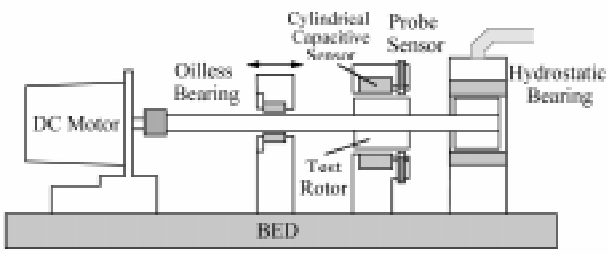

FIGURE 9: Experimental Setup

The whole schematic of experiment is shown in Fig. 9. One side of the rotor is supported with a hydrostatic bearing and the other side with an oilless bearing which can move along the axis. Orbit radius of the rotor is adjusted through altering both the rotating speed and the distance between the two bearings. Three different types of displacement sensors are used at the same time: probe type capacitive sensors (*PX405HA, LION PRECISION)*, existing 4-segment CCS, and newly designed 8-segment CCS. The photo of sensor housing

is shown in Fig.10. The 8-segment CCS and 4-segment CCS are molded inside the housing and the probe sensors are mounted at the holes.

In order to validate the performance of the new design of 8-segment CCS, special shapes of test rotors with 50 *mm* diameter are designed as shown in Fig.11. Rotor 1 is designed for the 3rd harmonic error, and rotor 2 is for the 4th harmonic error.

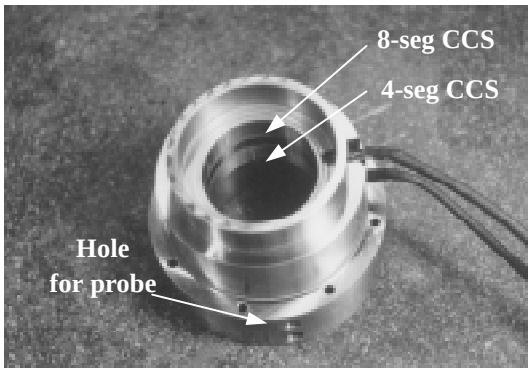

FIGURE 10: Sensor Housing

Practically, it is very difficult to materialize test rotors with certain harmonics of roundness error up to an accuracy of a few micrometers. However, the experiment need not be done with such rotors because the ratio of the eccentricity α to the magnitude of geometric error h is important, as shown in Eq. (7). This statement is valid in engineering sense if the gap δ between the rotor and the sensor is about ten times larger than the eccentricity and the magnitudes of geometric errors. Therefore, the gap δ is chosen as 500 μm, and test rotors are cut with the depth of 50 μm.

The main advantage of test rotors is that they possess not only 3rd and 4th harmonic errors but also multiples of them. Figure 12 shows the magnitudes of harmonic errors of test rotors. The zeroth harmonic component indicates the reduction in nominal radii of the test rotors.

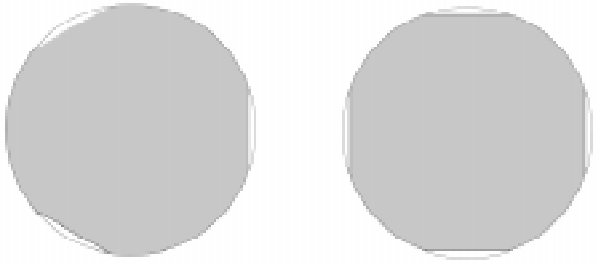

Rotor 1 Rotor 2

FIGURE 11: Test Rotors (Dia. 50 *mm*, Depth of cut 0.05 *mm*)

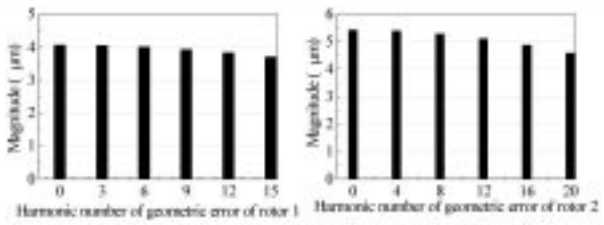

Rotor 1 Rotor 2

FIGURE 12: Magnitudes of Harmonic Errors of Test Rotors (Dia. 50 *mm*, Depth of cut 0.05 *mm*)

Experimental Results

Figure 13 gives the measured orbits with rotating error of 20 μm for rotor 1 and 30 μm for rotor 2. And Figure 14 is the corresponding spectrums. It is noticed in these two figures that multiples of the 3rd harmonic component remain in the measurement data of 2-probes and 4-probes, but CCS's are hardly affected by the roundness errors of the test rotors. This result validates the insensitivity of CCS to geometric errors.

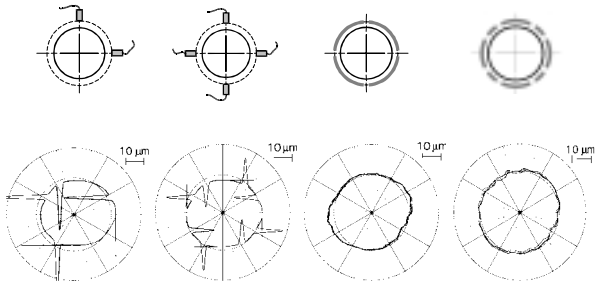

a) Rotor 1

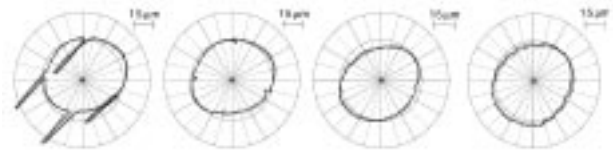

b) Rotor 2

FIGURE 13: Measured Orbits of Test Rotors with Various Sensor Type

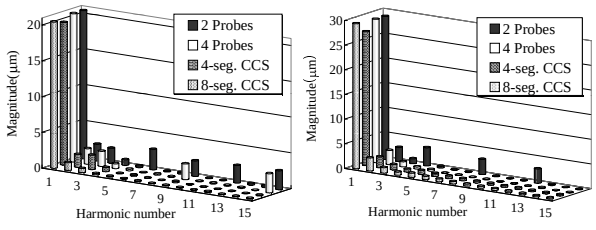

a) Rotor 1 a) Rotor 2

FIGURE 14: Spectrums of Measured Orbits

Figure 14 shows that multiples of the 4th harmonic component remain only in the 2 probes measurement data. This is because the differential configuration

rejects even harmonic components of the roundness error without regard to the sensor size, as mentioned before. There is little difference in the measurement data of 4-segment CCS and those of new 8-segment CCS in Fig.13, since the orbit radii are large compared to the magnitudes of roundness errors.

In order to compare the performances of two CCS's more clearly, experiments in the case of smaller orbit radii are performed. Figure 15 shows measured orbits with rotating errors of 20 μm and 10 μm. The smaller the rotating error, the more distorted the shape of orbit measured with the conventional 4-segment CCS. When the rotating error is about 5μm, i.e. nearly the same as the magnitude of the 3rd harmonic component, the effects of geometric errors become obvious. Conversely, measured orbits with the new 8-segment CCS maintain their circular shapes regardless of the rotating accuracy.

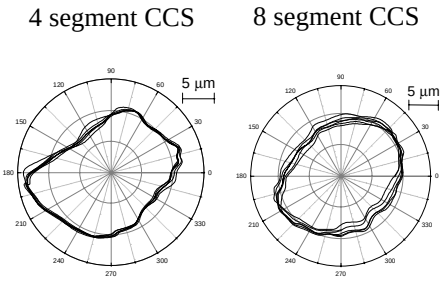

a) 10 μm orbit radius

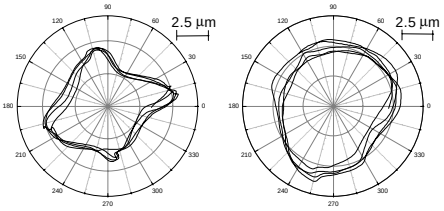

b) 5 μm orbit radius

FIGURE 15: Measured Orbits for Rotor 1 with the Conventional CCS and the New CCS

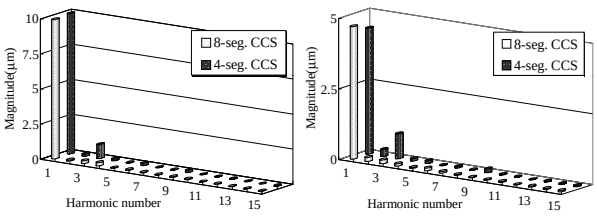

a) 10 μm orbit radius b) 5 μm orbit radius

FIGURE 16: Spectrums of Measured Data for Rotor 1 with the New CCS and the Conventional CCS

Spectrums in Fig.16 show that the distortions of the orbits of 4-segment CCS are caused by the 3rd harmonic component of geometric errors in the rotor, and the new 8-segment CCS filters the 3rd harmonic component very well.

CONCLUSION

Based on the error analysis of CCS, a new CCS with 8 sensing electrodes is proposed in this paper. New 8-segment CCS can reject not only the even harmonic error of rotor, but also an arbitrary odd harmonic error by changing the angular size of the CCS. The optimal abgular size of new CCS is obtained through minimizing 1-norm of error amplification factor. Experiments with test rotors verified the effectiveness of the new design. The new CCS is expected to reduce the elaboration of error seperation process in real-time feedback control system.

ACKNOWLEDGEMENT

This research was supported in part by a grant from the BK-21 Program for Mechanical and Aerospace Engineering Research at Seoul National University.

REFERENCES

1. Mitsui, K., Development of a New Measuring Method for Spindle Rotation Accuracy by Three-points Methods, *Proceedings of the 23rd int. MTDR*, pp. 115-121, 1982.
2. Gao, W., Kiyono, S. and Sugawara, T., Roundness Measurement by New Error Separation Method, *J. of Precision Engineering*, Vol. 21, pp. 123-132, 1997.
3. Chapman, P. D., A Capacitive based Ultraprecision Spindle Error Analyser, *J. of Precision Engineering*, Vol. 7, No. 3, July, pp. 129-137, 1985.
4. Chang, I. B., A Study on the Performance Improvement of a Magnetic Bearing System Using Built-in Capacitive Type Transducers, Ph.D Dissertation, Seoul National University, Korea, 1994.
5. Ahn, H. J., Jeon, S., and Han, D. C., Error Analysis of the Cylindrical Capacitive Sensor for Active Magnetic Bearing Spindles, ASME *J. of Dyn. Sys., Measurement, and Control*, Vol. 122, No. 1, March, pp.102-107, 2000.
6. Alexander H. Slocum, Precision Machine Design, Prentice-Hall, Inc., 1992.
7. Hammond Jr., J. L., and Glidewell, S. R., Design of Algorithms to Extract Data from Capacitance Sensors to Measure Fastener Hole Profiles, *IEEE Trans. Instr. Meas.*, Vol. 32, pp.343-349, 1983.